

Adaptive-scale damage detection strategy for plate structures based on wavelet finite element model

Wen-Yu He¹⁾ and *Songye Zhu²⁾

^{1), 2)} *Department of Civil and Environmental Engineering, The Hong Kong Polytechnic University, Hung Hom, Kowloon, Hong Kong, China*

²⁾ ceszhu@polyu.edu.hk

ABSTRACT

This study establishes an adaptive-scale damage detection strategy based on a wavelet finite element model (WFEM) for thin plate structures. Equations of motion and corresponding lifting schemes for thin plate structures are derived when the tensor products of cubic Hermite multi-wavelets are taken as the elemental interpolation functions. Sub-element damages are localized with the use of the change ratio of modal strain energy. Subsequently, such damages are adaptively quantified by using a damage quantification equation, which is deduced from differential equations of plate structure motion. WFEM scales are spatially varying and dynamically changing according to actual needs. Numerical examples clearly demonstrate that the proposed strategy can progressively locate and quantify plate damages. The strategy can operate efficiently in terms of the degrees-of-freedom in WFEM and sensors in the vibration test.

1. INTRODUCTION

Damage-induced changes of structural modal properties (such as frequencies, mode shapes, mode shape curvatures, and modal strain energy) are extensively used to locate and quantify structural damage (Doebling et al. 1996; Fan and Qiao 2011). Some of these damage detection methods rely on analytical structure models, such as finite element models (FEM), and they are referred to as model-based damage detection methods. Thin plates are common and important types of structural components in civil engineering, but relatively fewer studies have been conducted on plate elements than on 1D structural elements, such as truss, beam, and frame elements. Cornwell et al. (1999) derived a damage detection algorithm for plate-like structures on the basis of modal strain energy calculated from mode shapes before and after damage. Lee and Shin (2002) developed a damage identification algorithm for plates by using modal properties in the intact state and frequency response function in the damaged state. Yam et al. (2002) investigated the sensitivities of static and dynamic parameters to plate damage and provided recommendations for selecting damage indices in different cases. Wu and Law (2004) located plate damages by using

¹⁾ Graduate Student

²⁾ Associate Professor

the changes in uniform load surface curvature between intact and damaged states. Bayissa and Haritos (2007) identified plate damage by using a parameter derived from the power spectral density of bending moment response. This method can deal with both input–output and output-only problems. Hu and Wu (2009) presented a damage detection approach for plate structures based on experimental modal analysis and modal strain energy. Kazemi et al. (2010) proposed a plate damage identification method with two stages, namely, localization and quantification. This method is based on the variation in modal flexibility and artificial neural network technique. On the basis of elemental modal strain energy, Fan and Qiao (2012) presented a damage location factor matrix and severity correction factor matrix to locate and quantify damages in plate structures, respectively. Fu et al. (2013) developed a time domain response sensitivity-based FEM updating approach to identify local damages in plate structures.

Zhu et al. (2013; 2014) highlight the existing issue with FEM-based damage detection methods in that a delicate FEM with high spatial resolution can provide high-fidelity modal properties and enable the detection of minor damage, but it also results in high cost and difficulty in computation. Computation amounts increase exponentially along with degrees-of-freedom (DOFs) in FEM. Moreover, only low-order modal properties with limited accuracy are often identified through vibration testing, which makes delicate FEMs unnecessary. Therefore, a multi-scale FEM with high resolution at damage regions and relatively low resolution elsewhere is desirable to achieve an appropriate tradeoff between computation accuracy and efficiency (Zhu et al. 2013; 2014). They suggested that multi-scale FEM resolution adaptively changes according to detection progress: first, suspected damage regions are approximately identified by using a low-resolution model, and subsequently accurate results are obtained with local refinement in suspected regions.

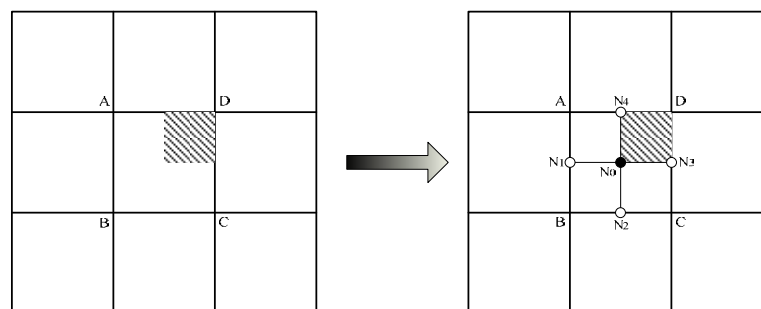


Fig. 1 Local refinement in traditional plate elements

However, implementing multi-scale models in the context of traditional FEMs involves reconstructing system matrices and repeating the entire computation process after remeshing local suspected damage regions (He and Zhu 2013). The process becomes even more complicated for plate structures. Fig. 1 shows a plate with a damaged region, which is represented by the shaded area. The plate is initially divided into nine elements. If the center element (ABCD) is identified as a suspected damage region, such element is subsequently divided into four equal elements. In the subsequent refinement, one node (N0) is introduced inside the element and four hanging nodes on the elemental edges (N1 to N4). These hanging nodes need to meet

special compatibility conditions and may cause numerical computation difficulties (Becker and Braack 2000; Biboulet et al. 2013).

Zhu et al. (2013; 2014) proposed an adaptive-scale damage detection strategy for beam structures using wavelet finite element model (WFEM) to resolve the abovementioned dilemma. WFEM has been proven to have superior multi-resolutions and localization properties (Ko et al. 1995; Amaratunga and Sudarshan 2006; He et al. 2012; He and Ren 2013; Li and Chen 2014). This strategy locates and quantifies structural damages in a progressive manner. WFEM employs a coarse model to identify likely damaged regions and then estimates accurate damage information with local refinement. In this study, the adaptive damage detection strategy is extended from 1D beam elements to 2D thin plate elements. Dynamical equations and corresponding lifting schemes for thin plate structures are derived using the tensor products of cubic Hermite multi-wavelets, which are used as the elemental shape functions. Consequently, sub-element damage can be located through change ratios of modal strain energy and progressively quantified by using a damage quantification equation deduced from differential motion equations. WFEM scales are adaptively lifted or reduced according to actual needs during detection. Consequently, appropriate tradeoffs between modeling details and integrity, as well as between computation accuracy and efficiency, are ideally achieved. The effectiveness and advantages of the proposed adaptive-scale damage detection strategy are verified through the numerical examples of simulated plate structures with single and double damages.

2. MULTI-SCALE WFEM FOR THIN PLATE STRUCTURES

Multi-scale WFEMs are fundamental to the proposed adaptive-scale damage detection strategy for plate structures. Such models employ scaling or wavelet functions as elemental shape functions. A variety of wavelet plate elements have been developed by using different wavelet types, such as spline wavelets (Chen and Wu 1995; Han et al. 2006), Daubechies wavelets (Diaz et al. 2009), B-spline wavelets (Xiang et al. 2008; Chen et al. 2010), trigonometric wavelets (He and Ren 2013), and Hermite wavelets (Wang and Wu 2013). The wavelet plate element based on second-generation cubic Hermite multi-wavelets (Wang and Wu 2013) is adopted for its favorable localization characteristics and convenient integral operation. The adaptive-scale detection strategy is extended to 2D thin plate structures in this section.

Scaling functions at scale 0 consist of two cubic Hermite splines are given by

$$\phi_{0,0} = [\phi_{0,0}^1(x) \quad \phi_{0,0}^2(x)] \quad (1)$$

where

$$\phi_{0,0}^1(x) = \begin{cases} (x+1)^2(-2x+1) & x \in [-1,0] \\ (x-1)^2(2x+1) & x \in [0,1] \\ 0 & \text{otherwise} \end{cases} \quad (2a)$$

$$\phi_{0,0}^2(x) = \begin{cases} (x+1)^2 x & x \in [-1, 0] \\ (x-1)^2 x & x \in [0, 1] \\ 0 & \text{otherwise} \end{cases} \quad (2b)$$

A simple form of cubic Hermite wavelet function at scale 0 (Averbuch et al. 2007) is expressed as

$$\psi_{0,0} = \phi_{1,0} \quad (3)$$

Spanning of scaling functions $\Phi_j = \{\Phi_j^1, \Phi_j^2\} = \{\phi_{j,k}^1, \phi_{j,k}^2 : k \in K(j)\}$ at scale j forms space V^j , where subscripts j and k define the scale and shift of the scaling function. Spanning of corresponding wavelet functions $\Psi_j = \{\Psi_j^1, \Psi_j^2\} = \{\psi_{j,m}^1, \psi_{j,m}^2 : m \in M(j)\}$ at scale j forms space W^j . The orthogonal complement of V^j is wavelet space W^j (i.e., $V^{j+1} = V^j \oplus W^j$ and $V^0 \subset V^1 \subset \dots \subset V^j \dots$). Details about cubic Hermite multi-wavelets are discussed in Zhu et al. (2013).

The 2D cubic Hermite wavelets of scale j are constructed by using the tensor products of 1D wavelets (Wang and Wu 2013; Quraishi and Sandeep 2013), it consists four functions

$$\bar{\Phi}_j^1(x, y) = \Phi_j^1(x) \otimes \Phi_j^1(y) \quad (4a)$$

$$\bar{\Phi}_j^2(x, y) = \Phi_j^1(x) \otimes \Phi_j^2(y) \quad (4b)$$

$$\bar{\Phi}_j^3(x, y) = \Phi_j^2(x) \otimes \Phi_j^1(y) \quad (4c)$$

$$\bar{\Phi}_j^4(x, y) = \Phi_j^2(x) \otimes \Phi_j^2(y) \quad (4d)$$

These functions stand the displacement, horizontal difference, vertical difference, and diagonal difference of the displacement field respectively. The two-dimensional wavelet at the scale $j = 1$ are shown in Fig.2. Spanning of scaling functions $\bar{\Phi}_j = \{\bar{\Phi}_j^1, \bar{\Phi}_j^2, \bar{\Phi}_j^3, \bar{\Phi}_j^4\}$ at scale j forms space F^j , which also has the multi-resolution property, i.e. $F^0 \subset F^1 \subset \dots \subset F^j$, $F^{j+1} = F^j \oplus G^j$, G^j is spanned by the corresponding 2D wavelet functions $\bar{\Psi}_j$ of scale j , which also has a simple form

$$\bar{\Psi}_j = \bar{\Phi}_{j+1} \quad (5)$$

According to classical Kirchoff–Love plate theory, the generalized function of potential energy of an elastic rectangular thin plate with dimensions l_x by l_y is (Zienkiewicz and Taylor 1961)

$$\Pi_p = \frac{1}{2} \iint_{\Omega} \kappa^T \mathbf{D} \kappa dx dy - \frac{1}{2} \iint_{\Omega} \rho t \lambda w^2 dx dy \quad (6)$$

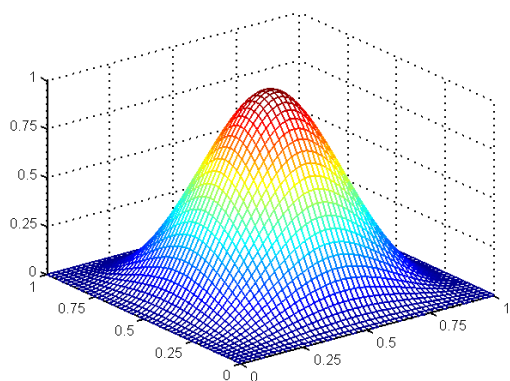
where Ω is the solving domain, w is the displacement field function, and λ is the vibration eigenvalues, κ is the generalized strain matrix, and \mathbf{D} is the plate elasticity matrix. These parameters are defined as follows:

$$\kappa = \left[-\frac{\partial^2 w}{\partial x^2} \quad -\frac{\partial^2 w}{\partial y^2} \quad -\frac{\partial^2 w}{\partial x \partial y} \right]^T \quad (7)$$

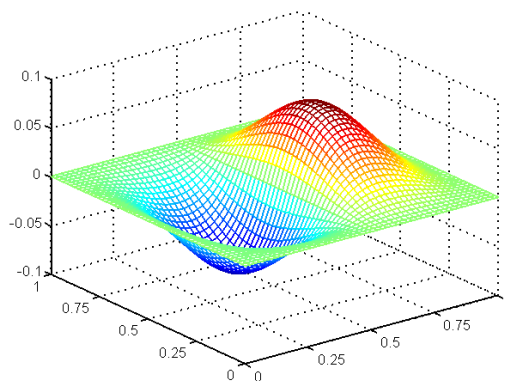
$$\mathbf{D} = D_0 \begin{bmatrix} 1 & \nu & 0 \\ \nu & 1 & 0 \\ 0 & 0 & (1-\nu)/2 \end{bmatrix} \quad (8)$$

$$D_0 = \frac{Et^3}{12(1-\nu^2)} \quad (9)$$

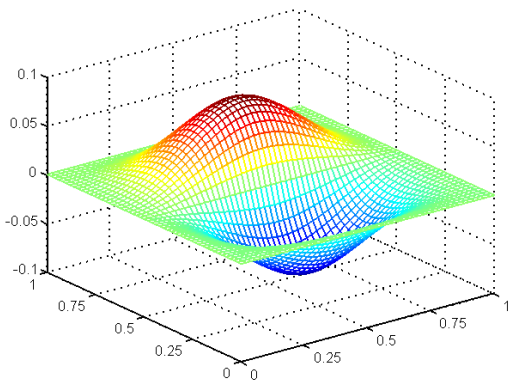
where ν denotes Poisson's ratio.



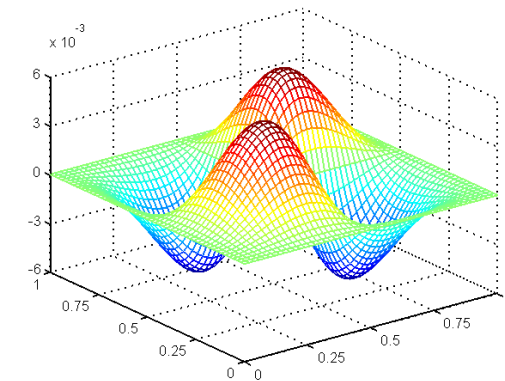
(a) Scaling function $\bar{\Phi}_1^1$



(b) Scaling function $\bar{\Phi}_1^2$



(c) Scaling function $\bar{\Phi}_1^3$



(d) Scaling function $\bar{\Phi}_1^4$

Fig. 2 2D tensor products of cubic Hermite functions

By using 2D multi-wavelet $\bar{\Phi}_j$ as the shape function and translating the corresponding coordinate into a standard solving domain, the unknown displacement field function $w(\xi, \eta)$ is expressed as:

$$w(\xi, \eta) = \bar{\Phi}_0 \mathbf{a}_0 + \sum_{n=0}^{j-1} \bar{\Psi}_n \mathbf{b}_n = \bar{\Phi}_j \mathbf{q}_j \quad (10)$$

where ξ and η represent local coordinates, $\bar{\Phi}_0$ represents scaling functions at scale 0, $\bar{\Phi}_j = [\bar{\Phi}_0 \bar{\Psi}_0 \bar{\Psi}_1 \cdots \bar{\Psi}_{j-1}]$ represents wavelet functions at scale j , \mathbf{q}_j is the undetermined vector of wavelet coefficients (i.e., coordinates corresponding to wavelet DOFs). Mode shapes expressed in general DOFs can be conveniently converted into wavelet DOFs using interpolation properties of adopted multi-wavelets.

According to the minimum potential energy principle, substitute Eq. (10) into Eq. (6) and let $\delta\Pi_p = 0$, where δ is the variational operator. The wavelet formulations for the free vibration of elastic thin plates are then obtained as

$$(\mathbf{K}_j - \lambda\mathbf{M}_j)\mathbf{q}_j = 0 \quad (11)$$

where \mathbf{M}_j and \mathbf{K}_j are the element mass and stiffness matrices at scale j .

$$\mathbf{M}_j = l_x l_y \rho t \Gamma_1^{j,0,0} \otimes \Gamma_2^{j,0,0} \quad (12)$$

$$\mathbf{K}_j = D_0 \left[\Gamma_1^{j,2,2} \otimes \Gamma_2^{j,0,0} + \nu \Gamma_1^{j,0,2} \otimes \Gamma_2^{j,2,0} + \Gamma_1^{j,0,0} \otimes \Gamma_2^{j,0,0} + 2(1-\nu) \Gamma_1^{j,1,1} \otimes \Gamma_2^{j,1,1} \right] \quad (13)$$

$$\Gamma_1^{j,2,2} = \frac{1}{l_x^3} \int_0^1 (\Phi_j'')^T \Phi_j'' d\xi = \frac{1}{l_x^3} \int_0^1 \begin{bmatrix} (\Phi_0'')^T \Phi_0'' & (\Phi_0'')^T \Psi_0'' & \cdots & (\Phi_0'')^T \Psi_{j-1}'' \\ & (\Psi_0'')^T \Psi_0'' & \cdots & (\Psi_0'')^T \Psi_{j-1}'' \\ \text{sym} & & \ddots & \vdots \\ & & & (\Psi_{j-1}'')^T \Psi_{j-1}'' \end{bmatrix} d\xi \quad (14)$$

$$\Gamma_1^{j,0,2} = \frac{1}{l_x} \int_0^1 \Phi_j^T \Phi_j'' d\xi = \frac{1}{l_x} \int_0^1 \begin{bmatrix} \Phi_0^T \Phi_0'' & \Phi_0^T \Psi_0'' & \cdots & \Phi_0^T \Psi_{j-1}'' \\ & \Psi_0^T \Psi_0'' & \cdots & \Psi_0^T \Psi_{j-1}'' \\ \text{sym} & & \ddots & \vdots \\ & & & \Psi_{j-1}^T \Psi_{j-1}'' \end{bmatrix} d\xi \quad (15)$$

$$\Gamma_1^{j,2,0} = (\Gamma_1^{j,0,2})^T \quad (16)$$

$$\Gamma_1^{j,1,1} = \frac{1}{l_x} \int_0^1 (\Phi_j')^T \Phi_j' d\xi = \frac{1}{l_x} \int_0^1 \begin{bmatrix} (\Phi_0')^T \Phi_0' & (\Phi_0')^T \Psi_0' & \cdots & (\Phi_0')^T \Psi_{j-1}' \\ & (\Psi_0')^T \Psi_0' & \cdots & (\Psi_0')^T \Psi_{j-1}' \\ \text{sym} & & \ddots & \vdots \\ & & & (\Psi_{j-1}')^T \Psi_{j-1}' \end{bmatrix} d\xi \quad (17)$$

$$\Gamma_1^{j,0,0} = l_x \int_0^1 \Phi_j^T \Phi_j d\xi = l_x \int_0^1 \begin{bmatrix} \Phi_0^T \Phi_0 & \Phi_0^T \Psi_0 & \cdots & \Phi_0^T \Psi_{j-1} \\ & \Psi_0^T \Psi_0 & \cdots & \Psi_0^T \Psi_{j-1} \\ \text{sym} & & \ddots & \vdots \\ & & & \Psi_{j-1}^T \Psi_{j-1} \end{bmatrix} d\xi \quad (18)$$

where Φ_j'' and Φ_j' represent the second and first derivatives with respect to local coordinate ξ , respectively. Integrals $\Gamma_2^{j,f,g}$ ($f, g = 0, 1, 2$) are similar to $\Gamma_1^{j,f,g}$ ($f, g = 0, 1, 2$), and only l_x and $d\xi$ have to be replaced by l_y and $d\eta$, respectively.

Lifting or lowering procedures between scales result in slight changes in the matrices. Matrices of the current scale [i.e., Eqs. (14) to (18)] are mainly retained, and only a few rows and columns need to be added or deleted. Although scale lifting or lowering procedures are analogous to mesh refinement or roughening processes in traditional FEM, the former procedures have simpler operations because re-meshing structures and re-constructing whole matrices are not conducted. Furthermore, challenges associated with hanging nodes are avoided. This advantage considerably reduces computation costs of adaptive-scale damage detection, where modeling scales need to be dynamically changed according to actual needs.

3. ADAPTIVE-SCALE DAMAGE DETECTION

Damage detection based on modal strain energy has been extensively explored in the context of traditional FEM (e.g., Shi and Law 1998; Cornwell et al. 1999; Guan and Karbhari 2008; Yan et al. 2010). Thanks to the multi-scale features of WFEM, modal strain energy in the proposed adaptive-scale damage detection strategy can be computed not only for elements but also for sub-elements. This enables this strategy to identify the damage with a size smaller than an element. Therefore, partial differential equations governing plate free vibrations are formulated for sub-elements in this section. Consequently, a damage quantification equation is derived.

3.1 Damage localization

According to Cornwell et al. (1999), the modal strain energy of an element or sub-element A_r associated with the i^{th} mode shape of a plate is

$$MSE_{i,r} = \frac{1}{2} \iint_{A_r} D_0(x, y) \left[\left(\frac{\partial^2 \varphi_i}{\partial x^2} \right)^2 + \left(\frac{\partial^2 \varphi_i}{\partial y^2} \right)^2 + 2\nu \left(\frac{\partial^2 \varphi_i}{\partial x^2} \right) \left(\frac{\partial^2 \varphi_i}{\partial y^2} \right) + 2(1-\nu) \left(\frac{\partial^2 \varphi_i}{\partial x \partial y} \right)^2 \right] dx dy \quad (19)$$

$$MSE_{i,r}^d = \frac{1}{2} \iint_{A_r} D_0^d(x, y) \left[\left(\frac{\partial^2 \varphi_i^d}{\partial x^2} \right)^2 + \left(\frac{\partial^2 \varphi_i^d}{\partial y^2} \right)^2 + 2\nu \left(\frac{\partial^2 \varphi_i^d}{\partial x^2} \right) \left(\frac{\partial^2 \varphi_i^d}{\partial y^2} \right) + 2(1-\nu) \left(\frac{\partial^2 \varphi_i^d}{\partial x \partial y} \right)^2 \right] dx dy \quad (20)$$

where A_r represents the element or sub-element with damage; $MSE_{i,r}$ and $MSE_{i,r}^d$ represent the modal strain energy before and after damage, respectively; superscript d denotes the damaged state; and D_0 denotes element or sub-element bending rigidity. Intact D_0 is used as an approximation in Eq. (20) when bending rigidity after damage D_0^d is unknown. A normalized change ratio of modal strain energy is used as a damage location indicator:

$$NMSECR_r^i = \frac{|MSE_{i,r}^d - MSE_{i,r}|}{MSE_{i,r}} / \max\left(\frac{|MSE_{i,r}^d - MSE_{i,r}|}{MSE_{i,r}}\right) \quad (21)$$

The damage location indicator is defined as the average of $NMSECR_r^i$ for all modes of interest when more than one vibration mode shape is considered.

$$NMSECR_r = \frac{1}{m} \sum_{i=1}^m NMSECR_r^i \quad (22)$$

3.2 Damage quantification

Assuming that plate damage occurrence causes a change in bending rigidity,

$$D_0^d(x, y) = D_0(x, y) + \Delta D_0(x, y) = D_0(x, y) + \sum_r \beta_r D_0(x, y) \quad (-1 \leq \beta_r \leq 0) \quad (23)$$

where β_r is the damage index of sub-element A_r .

Damage causes small perturbations in the i^{th} eigenvalue and mode shape in comparison with those of undamaged plates.

$$\lambda_i^d = \lambda_i + \Delta \lambda_i \quad (24)$$

$$\varphi_i^d = \varphi_i + \Delta \varphi_i = \varphi_i + \sum_{s \neq i} p_{is} \varphi_s \quad (25)$$

where λ_i and λ_i^d are the eigenvalues before and after damage, respectively; and φ_i and φ_i^d are the mode shapes before and after damage, respectively. Change in the i^{th} mode shape $\Delta \varphi_i$ is expressed as a linear combination of mode shapes other than the present one. According to Clough and Penzien (1993), the partial differential equation defining eigensolutions of the undamaged plate is:

$$D_0 \left[\frac{\partial^4 \varphi_i}{\partial x^4} + 2 \frac{\partial^4 \varphi_i}{\partial x^2 \partial y^2} + \frac{\partial^4 \varphi_i}{\partial y^4} \right] - \lambda_i m(x, y) \varphi_i = 0 \quad (26)$$

When the plate is subject to damage, Eq. (26) with small perturbation becomes:

$$[D_0 + \Delta D_0] \left[\frac{\partial^4 (\varphi_i + \Delta \varphi_i)}{\partial x^4} + 2 \frac{\partial^4 (\varphi_i + \Delta \varphi_i)}{\partial x^2 \partial y^2} + \frac{\partial^4 (\varphi_i + \Delta \varphi_i)}{\partial y^4} \right] - (\lambda_i + \Delta \lambda_i) m(\varphi_i + \Delta \varphi_i) = 0 \quad (27)$$

Substituting Eq. (26) into Eq. (27) and neglecting small terms leads to:

$$D_0 \left[\frac{\partial^4 \Delta \varphi_i}{\partial x^4} + 2 \frac{\partial^4 \Delta \varphi_i}{\partial x^2 \partial y^2} + \frac{\partial^4 \Delta \varphi_i}{\partial y^4} \right] + \Delta D_0 \left[\frac{\partial^4 \varphi_i}{\partial x^4} + 2 \frac{\partial^4 \varphi_i}{\partial x^2 \partial y^2} + \frac{\partial^4 \varphi_i}{\partial y^4} \right] - \lambda_i m \Delta \varphi_i - \Delta \lambda_i m \varphi_i = 0 \quad (28)$$

By pre-multiplying $\varphi_s (s \neq i)$ and computing the integral along the solving domain on both sides of Eq. (28) considering orthogonal conditions, coefficient p_{is} is computed as:

$$p_{is} = \frac{1}{\lambda_i - \lambda_s} \iint_{\Omega} \Delta D_0 \left(\frac{\partial^4 \varphi_i}{\partial x^4} + 2 \frac{\partial^4 \varphi_i}{\partial x^2 \partial y^2} + \frac{\partial^4 \varphi_i}{\partial y^4} \right) \varphi_s dx dy \quad (29)$$

Damage-induced changes in $MSE_{i,r}$ are expressed in two ways

$$\begin{aligned} \Delta MSE_{i,r} &= MSE_{i,r}^d - MSE_{i,r} \\ &= \iint_{A_r} D_0 \left[\frac{\partial^2 \varphi_i}{\partial x^2} \cdot \frac{\partial^2 \Delta \varphi_i}{\partial x^2} + \frac{\partial^2 \varphi_i}{\partial y^2} \cdot \frac{\partial^2 \Delta \varphi_i}{\partial y^2} + 2\nu \left(\frac{\partial^2 \varphi_i}{\partial x^2} \cdot \frac{\partial^2 \Delta \varphi_i}{\partial y^2} + \frac{\partial^2 \varphi_i}{\partial y^2} \cdot \frac{\partial^2 \Delta \varphi_i}{\partial x^2} \right) + 2(1-\nu) \frac{\partial^2 \varphi_i}{\partial x \partial y} \cdot \frac{\partial^2 \Delta \varphi_i}{\partial x \partial y} \right] dx dy \\ &+ \frac{1}{2} \iint_{A_r} \Delta D_0 \left[\left(\frac{\partial^2 \varphi_i}{\partial x^2} \right)^2 + \left(\frac{\partial^2 \varphi_i}{\partial y^2} \right)^2 + 2\nu \frac{\partial^2 \varphi_i}{\partial x^2} \cdot \frac{\partial^2 \varphi_i}{\partial y^2} + 2(1-\nu) \left(\frac{\partial^2 \varphi_i}{\partial x \partial y} \right)^2 \right] dx dy \end{aligned} \quad (30)$$

$$\begin{aligned} \Delta MSE_{i,r} &= MSE_{i,r}^d - MSE_{i,r} \\ &= \frac{1}{2} \iint_{A_r} D_0 \left[\left(\frac{\partial^2 \varphi_i^d}{\partial x^2} \right)^2 + \left(\frac{\partial^2 \varphi_i^d}{\partial y^2} \right)^2 + 2\nu \left(\frac{\partial^2 \varphi_i^d}{\partial x^2} \right) \left(\frac{\partial^2 \varphi_i^d}{\partial y^2} \right) + 2(1-\nu) \left(\frac{\partial^2 \varphi_i^d}{\partial x \partial y} \right)^2 \right] dx dy \\ &+ \frac{1}{2} \iint_{A_r} \Delta D_0 \left[\left(\frac{\partial^2 \varphi_i^d}{\partial x^2} \right)^2 + \left(\frac{\partial^2 \varphi_i^d}{\partial y^2} \right)^2 + 2\nu \left(\frac{\partial^2 \varphi_i^d}{\partial x^2} \right) \left(\frac{\partial^2 \varphi_i^d}{\partial y^2} \right) + 2(1-\nu) \left(\frac{\partial^2 \varphi_i^d}{\partial x \partial y} \right)^2 \right] dx dy \\ &- \frac{1}{2} \iint_{A_r} D_0 \left[\left(\frac{\partial^2 \varphi_i}{\partial x^2} \right)^2 + \left(\frac{\partial^2 \varphi_i}{\partial y^2} \right)^2 + 2\nu \left(\frac{\partial^2 \varphi_i}{\partial x^2} \right) \left(\frac{\partial^2 \varphi_i}{\partial y^2} \right) + 2(1-\nu) \left(\frac{\partial^2 \varphi_i}{\partial x \partial y} \right)^2 \right] dx dy \end{aligned} \quad (31)$$

Supposing there are l elements or sub-elements of a plate are localized as damaged regions by $NCRMSE$ as described in Section 3.1, the following damage quantification equation is obtained from Eqs. (29) and (31):

$$\begin{bmatrix} \chi_{11} & \chi_{12} & \cdots & \chi_{1l} \\ \chi_{21} & \chi_{22} & \cdots & \chi_{2l} \\ \vdots & \vdots & & \vdots \\ \chi_{l1} & \chi_{l2} & \cdots & \chi_{ll} \end{bmatrix} \begin{Bmatrix} \beta_1 \\ \beta_2 \\ \vdots \\ \beta_l \end{Bmatrix} = \begin{Bmatrix} \Delta E_{i,1} \\ \Delta E_{i,2} \\ \vdots \\ \Delta E_{i,l} \end{Bmatrix} \quad (32)$$

where

$$\begin{aligned} \chi_{mm} &= \sum_{s \neq i} P_{is} \iint_{\Delta A_m} \left[\frac{\partial^2 \varphi_i}{\partial x^2} \frac{\partial^2 \varphi_s}{\partial x^2} + \frac{\partial^2 \varphi_i}{\partial y^2} \frac{\partial^2 \varphi_s}{\partial y^2} + 2\nu \left(\frac{\partial^2 \varphi_i}{\partial x^2} \frac{\partial^2 \varphi_s}{\partial y^2} + \frac{\partial^2 \varphi_i}{\partial y^2} \frac{\partial^2 \varphi_s}{\partial x^2} \right) + 2(1-\nu) \frac{\partial^2 \varphi_i}{\partial x \partial y} \frac{\partial^2 \varphi_s}{\partial x \partial y} \right] dx dy \\ &+ \frac{1}{2} \iint_{\Delta A_m} D_0 \left[\left(\frac{\partial^2 \varphi_i}{\partial x^2} \right)^2 + \left(\frac{\partial^2 \varphi_i}{\partial y^2} \right)^2 + 2\nu \left(\frac{\partial^2 \varphi_i}{\partial x^2} \right) \left(\frac{\partial^2 \varphi_i}{\partial y^2} \right) + 2(1-\nu) \left(\frac{\partial^2 \varphi_i}{\partial x \partial y} \right)^2 \right] dx dy \\ &- \frac{1}{2} \iint_{\Delta A_m} D \left[\left(\frac{\partial^2 \varphi_i^d}{\partial x^2} \right)^2 + \left(\frac{\partial^2 \varphi_i^d}{\partial y^2} \right)^2 + 2\nu \left(\frac{\partial^2 \varphi_i^d}{\partial x^2} \right) \left(\frac{\partial^2 \varphi_i^d}{\partial y^2} \right) + 2(1-\nu) \left(\frac{\partial^2 \varphi_i^d}{\partial x \partial y} \right)^2 \right] dx dy \end{aligned} \quad (33)$$

$$\chi_{mn} = \sum_{i \neq s} P_{is} \iint_{\Delta A_m} \left[\frac{\partial^2 \varphi_i}{\partial x^2} \frac{\partial^2 \varphi_s}{\partial x^2} + \frac{\partial^2 \varphi_i}{\partial y^2} \frac{\partial^2 \varphi_s}{\partial y^2} + 2\nu \left(\frac{\partial^2 \varphi_i}{\partial x^2} \frac{\partial^2 \varphi_s}{\partial y^2} + \frac{\partial^2 \varphi_i}{\partial y^2} \frac{\partial^2 \varphi_s}{\partial x^2} \right) + 2(1-\nu) \frac{\partial^2 \varphi_i}{\partial x \partial y} \frac{\partial^2 \varphi_s}{\partial x \partial y} \right] dx dy \quad (34)$$

$$\begin{aligned} \Delta E_{i,m} = & \frac{1}{2} \iint_{\Delta A_m} D_0 \left[\left(\frac{\partial^2 \varphi_i^d}{\partial x^2} \right)^2 + \left(\frac{\partial^2 \varphi_i^d}{\partial y^2} \right)^2 + 2\nu \left(\frac{\partial^2 \varphi_i^d}{\partial x^2} \right) \left(\frac{\partial^2 \varphi_i^d}{\partial y^2} \right) + 2(1-\nu) \left(\frac{\partial^2 \varphi_i^d}{\partial x \partial y} \right)^2 \right] dx dy \\ & - \frac{1}{2} \iint_{\Delta A_m} D_0 \left[\left(\frac{\partial^2 \varphi_i}{\partial x^2} \right)^2 + \left(\frac{\partial^2 \varphi_i}{\partial y^2} \right)^2 + 2\nu \left(\frac{\partial^2 \varphi_i}{\partial x^2} \right) \left(\frac{\partial^2 \varphi_i}{\partial y^2} \right) + 2(1-\nu) \left(\frac{\partial^2 \varphi_i}{\partial x \partial y} \right)^2 \right] dx dy \end{aligned} \quad (35)$$

where $(1 \leq m \leq l, 1 \leq n \leq l)$. After the damage is located using the damage location indicator (Eq.(21)), it can be qualified by solving the damage quantification equation (Eq.(32)). This two-stage process, which includes localization and quantification, effectively reduces matrix size and minimizes computation costs.

3.3 Progressive damage detection

Zhu et al. (2014) proposed an adaptive-scale damage detection strategy for beam structures. This strategy is extended to plate structures in this study. A low-resolution WFEM model is used to approximate the potential location and damage severity. A multi-resolution model with local refinement in suspected regions is further used for accurate detection results. This strategy is efficient because WFEM is refined only in key locations and only a limited number of sensors are added for critical regions. The main steps of the adaptive-scale damage detection strategy are:

- Step 1: The mode shapes in damaged and undamaged states are determined through sensor measurement and multi-scale WFEM, respectively. The corresponding modal strain energy in each region is calculated.
- Step 2: The suspected damage region is located by using *NCRMSE*. The region is quantified by using the damage quantification equation.
- Step 3: High-scale wavelet terms are added to the suspected damage regions to refine the WFEM. Each considered region is divided into four sub-regions with the same size. More sensors are added to the corresponding regions of the plate when necessary.
- Step 4: Steps 1 to 3 are repeated until changes in the damage detection results after refinement are minimal.

4. NUMERICAL EXAMPLES

The effectiveness of the proposed adaptive-scale damage detection strategy is demonstrated through the numerical examples of thin plates supported on four corners. Fig. 3 shows the thin plate dimensions of 600 mm × 700 mm × 3 mm. The aluminum material has the following properties: elastic modulus $E = 68.9\text{GPa}$, density $\rho = 2700\text{kg/m}^3$, and Poisson's ratio $\nu = 0.27$. Table 1 shows two damage cases considered in this study, namely, single-damage and double-damage cases. Considering only lower modal properties are obtained accurately in practical vibration tests, the first mode shape is used in Section 4.1, whereas the first three mode shapes are used in Section 4.2. Modal shapes calculated by using a densely meshed traditional FEM are taken as measurement results.

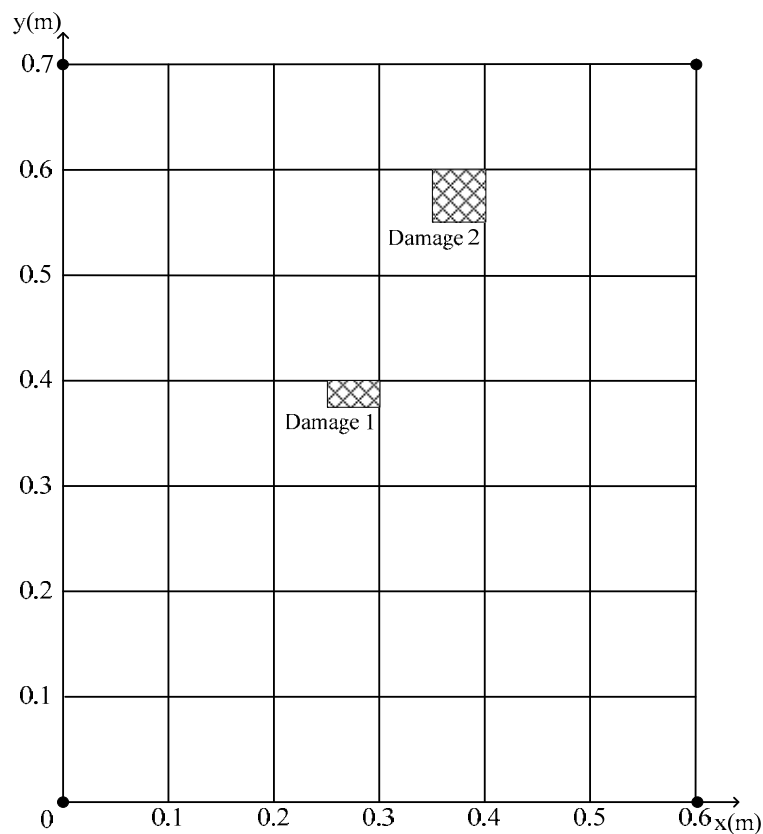


Fig. 3 Thin plate in numerical study

Table 1 Damage scenarios considered in the numerical study

Damage scenarios	Damage	
	Region	Severity (%)
Case 1	Damage 1 [0.200, 0.250] × [0.375, 0.400]	20
Case 2	Damage 1 [0.200, 0.250] × [0.375, 0.400]	20
	Damage 2 [0.350, 0.400] × [0.550, 0.600]	10

4.1 Examples without noise

Case 1 involves a single damage in the rectangle $[0.200, 0.250] \times [0.375, 0.400]$ with a 20% damage severity. Figs. 4 and 5 show the adaptive-scale model refinement process and corresponding damage localization results, respectively.

In Stage 1, the plate is first modeled by 6×7 wavelet plate elements at scale 0, that is, the displacement field function of each element is approximated in wavelet space F_0 . The corresponding number of DOFs at this stage is 220. Fig. 4 shows the damage location indicators associated with the first mode shape for each element. Fig. 5a shows region $[0.2, 0.3] \times [0.3, 0.4]$ (ABCD) as an identified suspected damage region. Table 2 describes the damage severity estimated by using the damage quantification

equation. As expected, the damage cannot be localized and quantified accurately because of the low-scale model. Subsequently, WFEM is refined in region ABCD by adding wavelets of scale 0 in Stage 2. In this stage, wavelet approximation space is lifted to F1. One more measurement point at (0.25, 0.35) is added to increase the resolution of the measured mode shape in region ABCD during the vibration test. Only the modal strain energy in suspected region ABCD is calculated. Fig. 5 shows the damage location identified in a smaller region $[0.25, 0.30] \times [0.35, 0.40]$ with improved estimation accuracy. Further refinement and identification processes were carried out for accurate detection results. In Stage 3, the wavelet approximation space in the suspected region is lifted to F2. Consequently, the suspected damage regions were further reduced to $[0.250, 0.275] \times [0.375, 0.400]$ and $[0.275, 0.300] \times [0.375, 0.400]$, which are identical to real damage regions in Fig.3. The refinement process is continued in Stage 4 by lifting the wavelet approximation space to F3 in suspected regions. Two more measurement points at (0.2625, 0.3875) and (0.2875, 0.3875) were added to the vibration test results. The suspected damage regions cannot be reduced further and results in Stages 3 and 4 in Fig.5 are almost the same. This implies that identified regions in Stage 3 are close to the real one and that no further refinement is necessary. Table 2 shows the corresponding damage quantification results using Eq. (32). The quantification accuracy of damage severity is effectively improved with the progressive refinement of WFEM. Such severity finally converges with real values in Stages 3 and 4. Damage severity quantification should only be conducted in the last stage to reduce the computation amount.

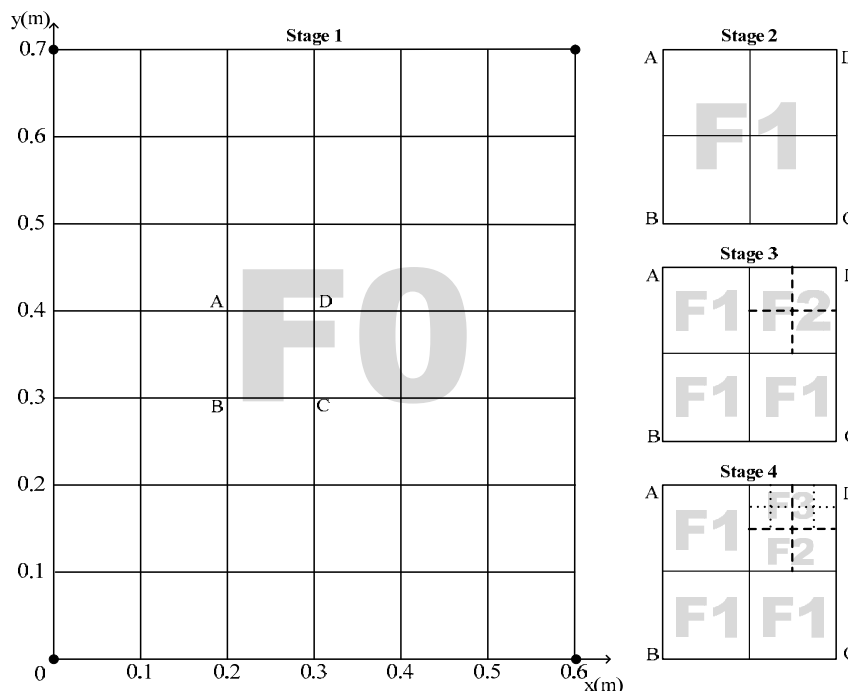


Fig. 4 Model refinement process in Case

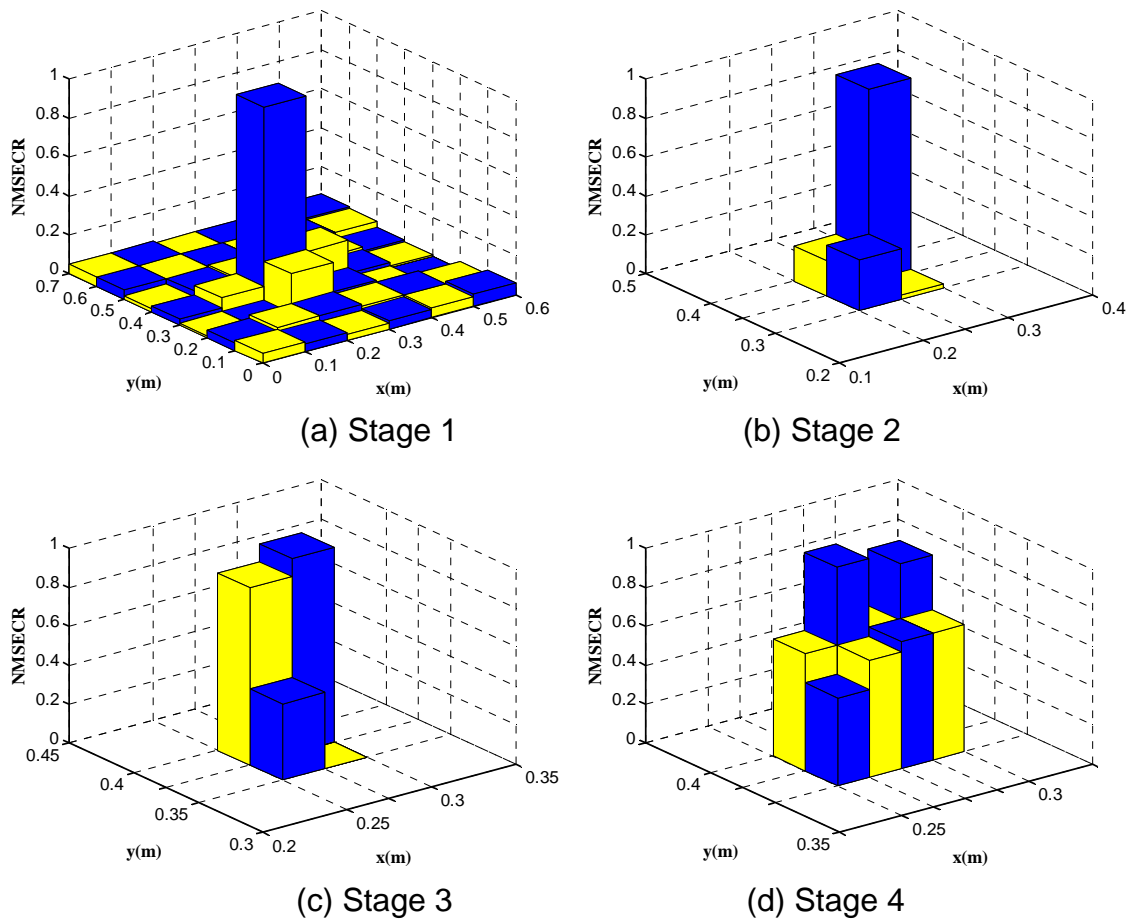


Fig. 5 Adaptive-scale damage identification results in Case 1

Table 1 and Fig. 3 show the double damages of Case 2: the first region $[0.200, 0.250] \times [0.375, 0.400]$ with 20% severity and the second region $[0.350, 0.400] \times [0.550, 0.600]$ with 10% severity. Following the similar process used in Case 1, the damage is progressively identified with improved accuracy. Fig.6, Fig.7 and Table 2 present the WFEM refinement process, damage localization, and quantification results, respectively.

Damage 2 consists of 1/168 of the entire plate. A good estimation of damage size and severity are obtained in Stage 2 and confirmed in Stage 3. Therefore, the wavelet approximation space was recovered to F1 in the Damage 2 region in Stage 4. Whereas Damage 1 consists of 1/336 of the plate and the relevant region is gradually refined until Stage 4. Therefore, the WFEM scale can be adaptively adjusted according to actual damage. This flexibility and adaptability enables the proposed strategy to achieve satisfactory damage detection results with minimized DOFs and computation costs. For example, using traditional FEM with uniform meshing in Case 1 requires at least 24×28 plate elements with 2,896 DOFs to capture damage location and severity accurately. Square plate elements are used because the actual damage region shape cannot be known in advance. However, only 236 DOFs are used in Stage 4 for Case 1 by using an adaptive-scale WFEM.

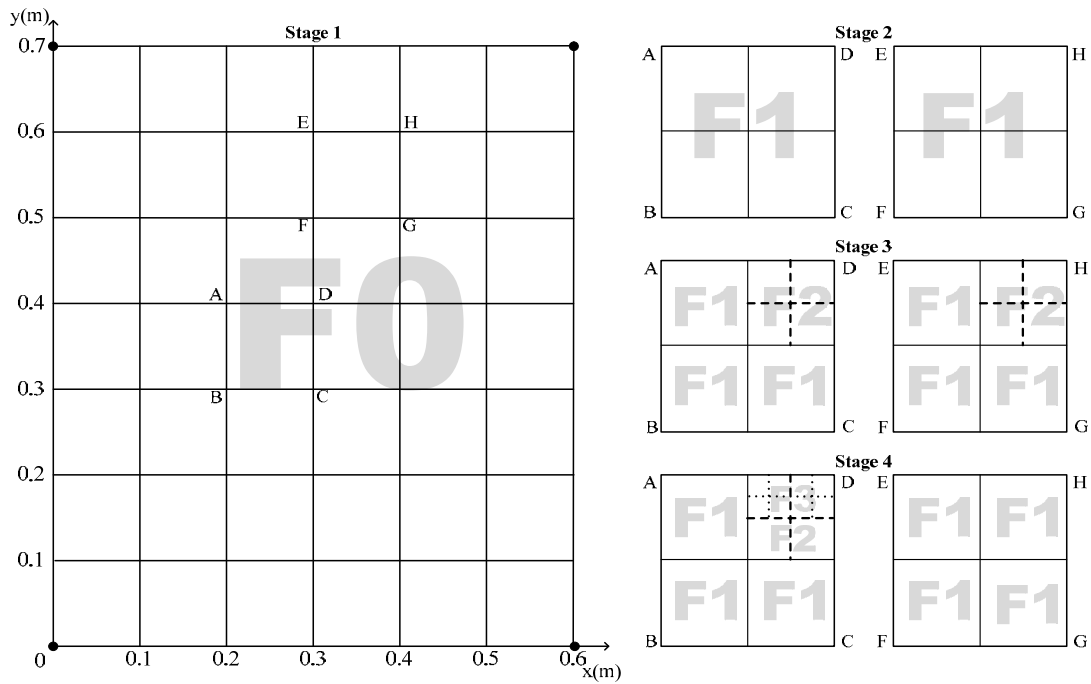


Fig. 6 Model refinement process in Case

Table 2 Damage severity quantification results (%)

Stage	Region	Case 1	Case 2
1	$[0.3000, 0.4000] \times [0.5000, 0.6000]$	/	2.8
	$[0.2000, 0.3000] \times [0.3000, 0.4000]$	2.8	2.5
2	$[0.3500, 0.4000] \times [0.5500, 0.6000]$	/	9.9
	$[0.2500, 0.3000] \times [0.3500, 0.4000]$	10.4	10.9
3	$[0.3500, 0.3750] \times [0.5500, 0.5750]$	/	9.8
	$[0.3500, 0.3750] \times [0.5750, 0.6000]$	/	10.0
	$[0.3750, 0.4000] \times [0.5500, 0.5750]$	/	9.8
	$[0.3750, 0.4000] \times [0.5750, 0.6000]$	/	9.9
	$[0.2500, 0.2750] \times [0.3750, 0.4000]$	19.1	19.1
	$[0.2750, 0.3000] \times [0.3750, 0.4000]$	18.9	18.9
	4	$[0.2500, 0.2625] \times [0.3750, 0.3875]$	18.4
$[0.2500, 0.2625] \times [0.3875, 0.4000]$		18.7	18.4
$[0.2625, 0.2750] \times [0.3750, 0.3875]$		20.0	19.8
$[0.2625, 0.2750] \times [0.3875, 0.4000]$		18.8	18.2
$[0.2750, 0.2850] \times [0.3750, 0.3875]$		18.8	18.2
$[0.2750, 0.2850] \times [0.3875, 0.4000]$		19.8	19.6
$[0.2850, 0.3000] \times [0.3750, 0.3875]$		18.2	17.6
	$[0.2850, 0.3000] \times [0.3875, 0.4000]$	18.4	19.5

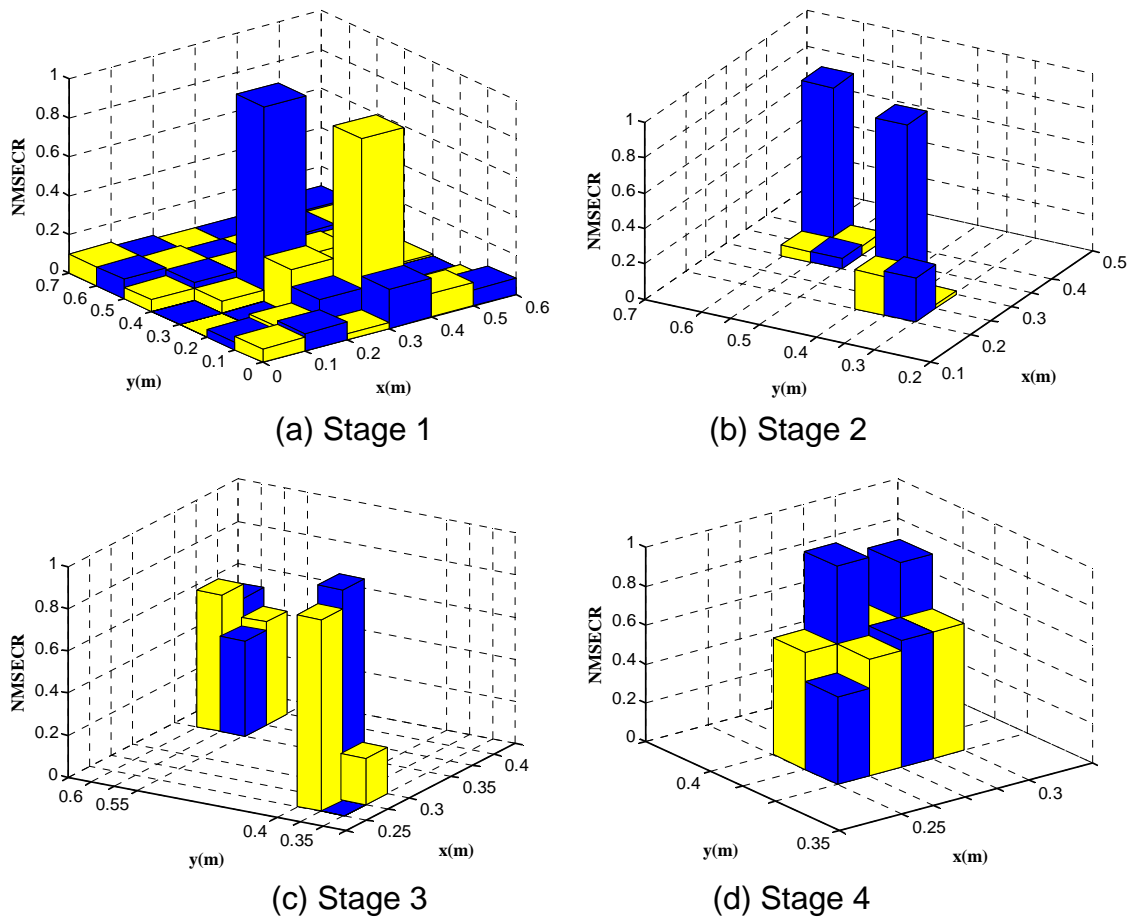


Fig. 7 Adaptive-scale damage identification results in Case 2

4.2 Examples with noise

Measurement noise contaminates the measured modal data in actual vibration tests. In this section, random error is added to measured mode shapes to consider measurement noise effect

$$\bar{\varphi}_{iz} = \varphi_{iz} (1 + \eta \zeta_{iz}) \quad (36)$$

where $\bar{\varphi}_{iz}$ and φ_{ij} are “measured” and accurate mode shape elements of the i th mode at z th DOF, respectively; η is the noise level; and ζ_{iz} is a zero-mean Gaussian random variable. Six different noise levels are considered: 0.5%, 1%, 1.5%, 2%, 2.5%, and 3%. A total of 1000 Monte Carlo simulations were performed for each noise level. The coefficient of variance (COV) is used to measure damage detection result variance:

$$COV = \sigma_{\Delta a} / \bar{a} \quad (37)$$

where \bar{a} and σ_a represent the mean and standard deviation of a distribution, respectively. A high COV implies that high uncertainty exists in a single sample or more samples are required to achieve accurate estimation.

The average damage location indicators and severity indices obtained from multiple vibration tests can well reflect actual structural damage locations and severity. This finding implies that average values from a sufficient number of testing results can minimize noise effects in damage detection. Fig.8a and Fig.8b show the COVs of estimated damage location indicators and severity indices in different scales in Case 1, respectively. Increases in COV, along with the measurement noise level, are apparent. Furthermore, uncertainty in detection results increases with the WFEM scale as well.

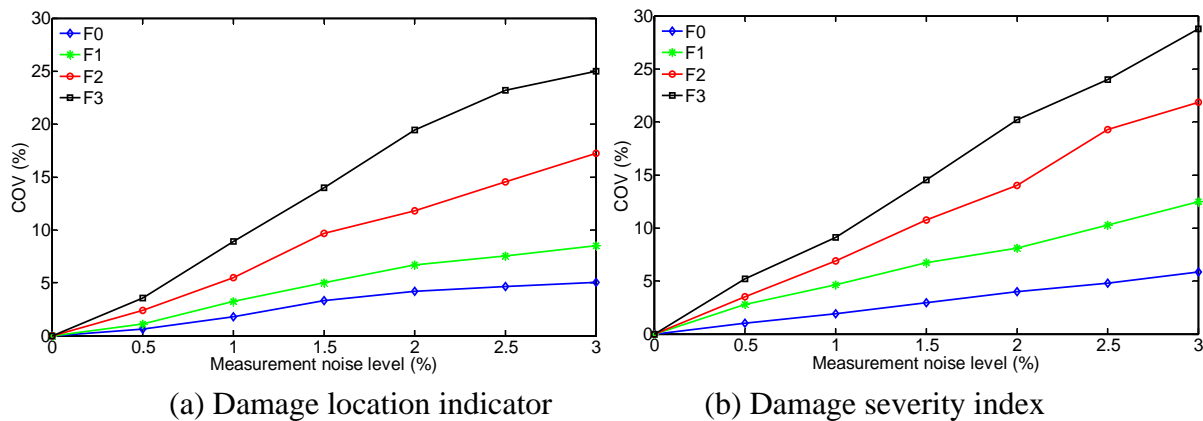


Fig. 8 COV of damage detection results in Case 1

5. CONCLUSIONS

A WFEM-based adaptive-scale damage detection strategy previously proposed for beam structures, is extended to thin plate structures in this study. Equations of motion and corresponding lifting schemes for thin plate structures are derived by using the tensor products of cubic Hermite multi-wavelets as elemental interpolation functions. Sub-element damages are located and quantified progressively during damage detection. WFEM is gradually refined from low to high resolution in critical regions. Therefore, the WFEM-based adaptive-scale damage detection strategy achieves a desirable tradeoff between modeling details and entirety. The numerical examples of thin plates supported on four corners demonstrate how the proposed strategy accurately and progressively detects damages. The proposed strategy is efficient in terms of DOFs, sensors, and computation efforts because the wavelet scale can be adaptively enhanced and reduced according to actual needs. Such refinement is necessary only for possible damage regions. The two-step detection process (i.e., localization and quantification) also improves the efficiency and accuracy of damage detection.

ACKNOWLEDGMENTS

The authors are grateful for the financial support from Research Institute for Sustainable Urban Development (Project No. 4-ZZCG) and from The Hong Kong Polytechnic University through (Project No. G-YL31). The findings and opinions expressed in this study are those of the authors alone and are unnecessarily the views of the sponsors.

REFERENCES

- Amaratunga, K. and Sudarshan, R. (2006), "Multi-resolution modeling with operator-customized wavelets derived from finite elements", *Comput Method Appl M*, **195** 2509-2532.
- Averbuch, A.Z., Zheludev, V.A. and Cohen, T. (2007) "Multiwavelet frames in signal space originated from Hermite splines", *IEEE T Signal Proces*, **55(3)** 797-808
- Bayissa, W.L. and Haritos, N. (2007) "Damage identification in plate-like structures using bending moment response power spectral density", *Struct Health Monit*, **6** 5-24
- Becker, R. and Braack, M. (2000) "Multigrid techniques for finite elements on locally refined meshes", *Numer Linear Algebr*, **7** 363-379
- Biboulet, N., Gravouil, A., Dureisseix, D., Lubrecht, A.A. and Combescure, A. (2013) "An efficient linear elastic FEM solver using automatic local grid refinement and accuracy control", *Finite Elem Anal Des*, **68** 23-38
- Chen, W.H. and Wu, C.W. (1995) "Spline wavelets element method for frame structures vibration", *Comput Mech*, **16** 1-21
- Chen, X.F., Xiang, J.W., Li, B. and He, Z.J. (2010) "A study of multiscale wavelet-based elements for adaptive finite element analysis", *Adv Eng Softw*, **41(2)** 196-205
- Clough, W. and Penzien, J. (1993) "Dynamics of Structures (third edition)", McGraw-Hill, New York
- Cornwell, P., Doebling, S.W. and Farrar, C.R. (1999) "Application of the strain energy damage detection method to plate-like structures", *J Sound Vib*, **224 (2)** 359-374
- Doebling, S.W., Farrar, C.R., Prime, M.B. and Shevitz, D.W. (1996) "Damage identification and health monitoring of structural mechanical systems from changes in their vibration characteristics: a literature review", Report No. LA-13070-MS, Los Alamos National Laboratory, Los Alamos, NM, USA
- Diaz, L.A., Martin, M.T. and Vampa, V. (2009) "Daubechies wavelet beam and plate finite elements", *Finite Elem Anal Des*, **45(3)** 200-209
- Fan, W. and Qiao, P.Z. (2011) "Vibration-based damage identification methods: a review and comparative study", *Struct Health Monit*, **10(1)** 83-111
- Fan, W. and Qiao, P.Z. (2012) "A strain energy-based damage severity correction factor method for damage identification in plate-type structures", *Mech Syst Signal Process*, **28** 660-678
- Fu, Y.Z., Lu, Z.R. and Liu, J.K. (2013) "Damage identification in plates using finite element model updating in time domain", *J Sound Vib*, **332** 7018-7032
- Guan, H. and Karbhari, V.M. (2008) "Improved damage detection method based on element modal strain damage index using sparse measurement", *J Sound Vib*,

309(3-5) 465-494

- Han, J.G., Ren, W.X. and Huang, Y. (2006) "A spline wavelet finite-element method in structural mechanics", *Int J Numer Meth Eng*, **66** 166-190
- He, W.Y. and Ren, W.X. (2012) "Finite element analysis of beam structures based on trigonometric wavelet", *Finite Elem Anal Des*, **51** 59-66
- He, W.Y. and Ren, W.X. (2013) "Adaptive trigonometric hermite wavelet finite element method for structural analysis", *Int J Struc Stab Dy*, **13(1)** 1350007
- He, W.Y., Ren, W.X. and Yang, Z.J. (2012) "Computation of plane crack stress intensity factors using trigonometric wavelet finite element methods", *Fatigue Frac Engng Mater Struct*, **35** 732-741
- He, W.Y. and Zhu, S. (2013) "Progressive damage detection based on multi-scale wavelet finite element model: numerical study", *Comput Struct*, **125** 177-186
- Hu, H. and Wu, C. (2009) "Development of scanning damage index for the damage detection of plate structures using modal strain energy method", *Mech Syst Signal Process*, **23** 274-287
- Kazemi, S., Fooladi, A. and Rahai, A.R. (2010) "Implementation of the modal flexibility variation to fault identification in thin plates", *Acta Astronaut*, **66** 414-426
- Ko, J., Kurdila, A.J. and Pilant, M.S. (1995) "A class of finite element methods based on orthonormal, compactly supported wavelets", *Compu. Mech*, **16** 235-244
- Lee, U. and Shin, J. (2002) "A structural damage identification method for plate structures", *Eng Struct*, **24** 1177-1188
- Li, B. and Chen, X.F. (2014) "Wavelet-based numerical analysis: A review and classification", *Finite Elem Anal Des*, **81** 14-31
- Quraishi, S.M. and Sandeep, K. (2013) "Multiscale modeling of beam and plates using customized second-generation wavelets", *J Eng Math*, **83** 185-202.
- Shi, Z.Y. and Law, S.S. (1998) "Structural damage localization from modal strain energy change", *J Sound Vib*, **218 (5)** 825-844
- Wang, Y.M. and Wu, Q. (2013) "Construction of operator-orthogonal wavelet-based elements for adaptive analysis of thin plate bending problems", *CMES-Comp Model Eng*, **93(1)** 17-45
- Wu, D., Law, S.S., (2004) "Damage localization in plate structures from uniform load surface curvature", *J Sound Vib*, **276** 227-244
- Xiang, J.W., Chen, X.F., He, Z.J. and Zhang, Y.H. (2008) "A new wavelet-based thin plate element using B-spline wavelet on the interval", *Comput Mech*, **41(2)** 243-255
- Yam, L.H., Li, Y.Y. and Wong, W.O. (2002) "Sensitivity studies of parameters for damage detection of plate-like structures using static and dynamic approaches", *Eng Struct*, **24** 1465-1475
- Yan, W.J., Huang, T.L. and Ren, W.X. (2010) "Damage detection method based on element modal strain energy sensitivity", *Adv Struct Eng*, **13** 1075-1088
- Zhu, S., He, W.Y. and Ren W.X. (2013) "Adaptive-scale damage detection for frame structures using beam-type wavelet finite element: experimental validation", *J Earthq Tsunami*, **7(3)** 1350024
- Zhu, S., He, W.Y. and Ren W.X. (2014) "A wavelet finite element-based adaptive-scale damage detection strategy", *Smart Struct Syst*, accepted
- Zienkiewicz, O.C. and Taylor, R.L. (1961) "The Finite Element Method", fourth ed., McGraw-Hill Book Company, London.